Rocky Worlds DDT: JWST Data Analysis Report for TOI-771 b

Ian Wong and Taylor J. Bell
JWST Data Analysis Team

June 26, 2026

1 Observation Overview

As part of the RWDDT program, JWST-DDT-12656 Observation 3 obtained time-series imaging of TOI-771 b on UT 2026 June 21–22 using the MIRI/F1500W filter with the BRIGHTSKY subarray, covering 2.56 hours. This was the third visit to the system, with the goal of measuring the secondary eclipse of the planet. The high-level science products (HLSPs) generated by our analyses are hosted on MAST and include both intermediate and final results to help drive research-community engagement.

We measured both the centroid position (x, y) and width of the target's point-spread function (PSF) during each integration; these are plotted in Figure 1. The telescope pointing remained quite stable along both the x and y axes throughout the observation. Meanwhile, the width of the PSF increased smoothly during the first $\sim$1 hour of the observation before settling at a mostly stable value for the remainder of the time series. This behavior is typical of time-series photometry obtained with MIRI.

2 Data Reduction

This report presents results from a reduction and analysis performed by Analyst Wong. The analysis used the standard JWST pipeline (`jwst` v1.20.2 with the CRDS context jwst_1464.pmap) for detector-level calibrations. Stage 1 processing included running the following steps: `dq_init`, `emicorr`, `saturation`, `firstframe`, `lastframe`, `reset`, `linearity`, `rscd`, `dark_current`, `jump` (with the threshold increased from 4.0 to 8.0), and `ramp fitting`. In Stage 2, we ran the `flat_field` step, but skipped the `photom` step as flux-calibrated data are not desired for time-series analyses.

Photometric extraction and light curve fitting were completed using Stages 3–5 of the `Eureka!` Python package (1.4.dev137+g7768b5cdd). In Stage 3, a time series was constructed for each pixel, and 5σ outliers (along with all NaN values) were replaced using bilinear interpolation over the nearest neighbors. The target's centroid position was iteratively calculated for each integration using the 'mgmc' center-of-mass centroiding method: a coarse initial guess was derived from the full subarray, followed by positional refinement from a 21×21 px cutout around the initial guess. The width of the target's PSF along the x and y axes was then measured in each integration by fitting a 2D Gaussian to the cutout region (see Figure 1). These measurements were compiled into cotrending vectors that were subsequently used as independent variables in the systematics modeling.

Photometric light curves were extracted in Stage 3 of `Eureka!` using the `photutils` package with circular apertures and 'exact' edges, where pixels are weighted by the fraction of their area lying within the specified aperture. A large grid of aperture size and

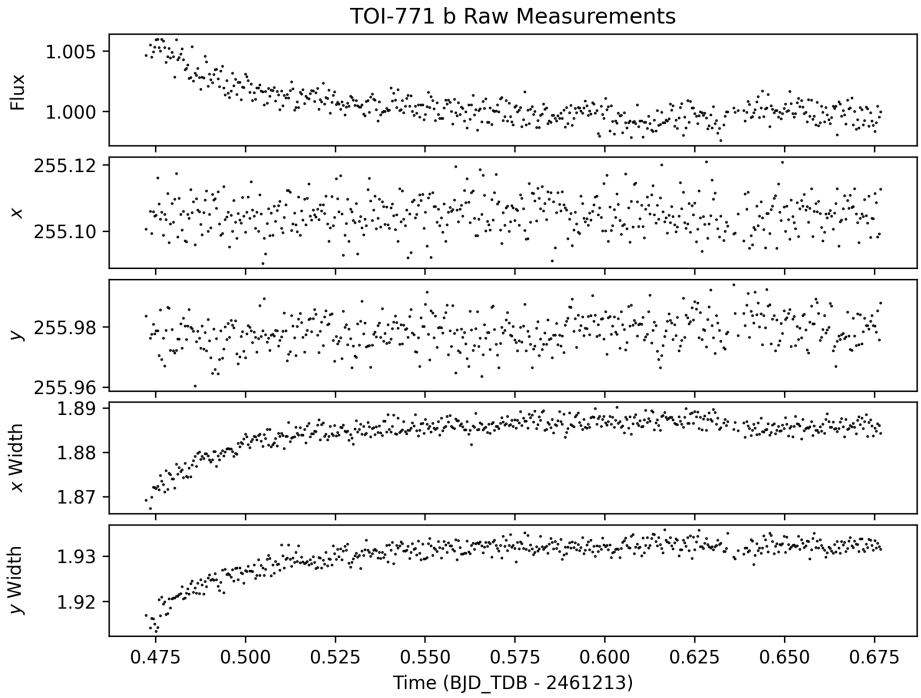

Figure 1: Measured flux and target centroid properties Time series of the relative changes in the normalized raw flux, centroid position (x, y), and PSF width (computed as the Gaussian standard deviation along the x and y axes), illustrating the initial settling behavior and overall stability of the telescope pointing and the PSF shape.

background region settings was employed to investigate the sensitivity of the eclipse fits to the photometric extraction parameters and determine a fiducial eclipse fit for this visit. Aperture radii ranged from 4–11 px, in 1 px steps. The inner radius of the background annulus varied from 14 to 26 px in 4 px steps, while the annulus width ranged from 10 to 30 px in 10 px steps. Photometric light curves were generated for each source aperture + background annulus pair. In Stage 4, we iteratively masked all integrations lying more than 3σ away from the rolling median computed using a boxcar filter with a width of 40 integrations.

3 Light Curve Fitting

A prominent feature in all of the extracted light curves is the significant decreasing ramp that spanned the first $\sim$1 hour of the observation. For the final set of runs carried out by Analyst Wong, the first 100 integrations were trimmed, which removed the steepest part of the ramp, while simultaneously preserving a long enough pre-eclipse baseline to adequately sample the out-of-eclipse flux level. The remaining ramp-like flux modulation was modeled using an exponential function in time.

To address instrumental systematics, the measured PSF centroid positions (x, y) and widths (sx, sy) were considered as linear detrending vectors and incorporated in our fits. Analyst Wong found that the inclusion of y was disfavored for all aperture settings when

considering the Bayes factor. The addition of a linear slope in time was also considered, but the best-fit slope value was consistent with zero across most aperture settings; in the fiducial fit presented in this report, the slope term was not included.

From Figure 1, it is evident that the measured light curve contains significant time-correlated flux modulations, particularly in the second half, which coincides with the predicted timing of the secondary eclipse of TOI-771 b. This correlated noise was not removed through systematics modeling using the linear detrending vectors and exponential ramp. The presence of this enhanced "red" noise can have a marked effect on the retrieved eclipse timing and depth from the fits. Analyst Wong experimented with modeling these temporal variations by including a `celerite2` Gaussian process (GP) with a Matérn-3/2 kernel as a function of time. The approximate Matérn-3/2 kernel as a function of time used as the GP model is defined as

$$k(t) = \sigma^2 \left[(1+1/\epsilon)\, e^{-(1-\epsilon)\sqrt{3}\,t/\rho}\,(1-1/\epsilon)\, e^{-(1+\epsilon)\sqrt{3}\,t/\rho}\right],$$

where $\epsilon = 0.1$ and controls the quality of `celerite2`'s approximation of the Matérn-3/2 kernel, ρ controls the length scale of the covariance (and is fitted in `Eureka!` with $m = \ln\rho$), and σ^2 controls the amplitude of the covariance (and is fitted in `Eureka!` with $A = \ln(\sigma^2)$).

We found that while the inclusion of a GP model did improve the noise characteristics of the resultant residuals, it tended to produce unphysically large eclipse depths (>700 ppm). This underscores the inherent impact of the red noise on the eclipse fit. In particular, we observed that the characteristic variability timescale of the best-fit GP models was typically comparable to or even shorter than the eclipse duration—a scenario that is especially susceptible to strong degeneracies between the GP model parameters and the mid-eclipse time and depth. In light of these findings, we chose to present results from our fit without a GP in this report.

All priors for the astrophysical and systematic models considered in our fiducial fit are summarized in Table 1. The full model can be summarized as:

$$\mathrm{Model}(t) = E(t) * S(t),$$

where $E(t)$ is the batman eclipse model, and $S(t)$ is the composite systematic noise model, defined as

$$S(t) = c_0 \left[1 + r_0 \exp\Big(-r_1(t - t_{\mathrm{start}})\Big)\right] X\Big(x(t)\Big) SX\Big(sx(t)\Big) SY\Big(sy(t)\Big), \tag{1}$$

where c_0 is a normalization factor, and r_0 and r_1 are parameters that characterize the decreasing exponential ramp, which is defined relative to the time of the first integration t_{start}. Each of X, SX, and SY is a linear decorrelation function, defined similarly to each other:

$$X\Big(x(t)\Big) = 1 + c_x\Big(x(t) - \overline{x}\Big),$$

where $x(t)$ is the measured centroid x position as a function of time, and ($sx(t)$, $sy(t)$) is the PSF width along the x and y axes as a function of time. The variable marked with the overline denotes the mean value of the respective array. Lastly, we also included a white

Table 1: The astrophysical and systematic model priors for the fits assuming a circular orbit. Fixed astrophysical parameters are shown without uncertainties and are taken from the circular fit from CIT's orbit fitting efforts during observational scheduling. Gaussian priors are shown as $\mathcal{N}(\mu, \sigma)$ with mean μ and standard deviation σ, while Uniform priors are shown as $\mathcal{U}(l, u)$ with lower-limit l and upper-limit u.

Parameter	Prior
P	2.3260184 d
$t_{\rm sec}$	$\mathcal{U}(2\,458\,573.58, 2\,458\,573.60)$ $\mathrm{BJD_{TDB}}$
b	0.1406
a/R_*	18.523
e	0
R_*[†]	0.232
$R_{\rm p}/R_*$	0.050153
$F_{\rm p}/F_*$	$\mathcal{U}(0, 1000)$ ppm
c_0	$\mathcal{N}(0.999, 0.01)$
c_x	$\mathcal{N}(0.0, 0.5)$
c_{sx}	$\mathcal{N}(0.0, 0.5)$
c_{sy}	$\mathcal{N}(0.0, 0.5)$
r_0	$\mathcal{N}(0.0, 0.01)$
r_1	$\mathcal{U}(3, 300)$
scatter_mult	$\mathcal{U}(0.8, 10)$

[†]The stellar radius is used to account for the difference in light travel time throughout the planet's orbit.

noise scaling factor, `scatter_mult`, as a multiplier to the photometric uncertainties estimated during the Stage 3 reduction.

All fits used the `dynesty` dynamic nested sampling algorithm. A multiplicative factor on the measured photometric uncertainties was included as a free parameter to ensure a final reduced chi-squared value of unity. For the fiducial analysis presented in this report, the sampling began with an initial set of 512 live points using the 'rwalk' sampling algorithm, the 'multi' bounds, and an initial stopping criterion of $d \log \mathcal{Z} < 0.01$, where $\mathcal{Z}$ is the Bayesian evidence. This initial sampling was then expanded by iteratively adding batches of live points with a 'pfrac' of 0.5 (which provides a balance between a precise posterior distribution and a precise Bayesian evidence) until the default stopping criterion was achieved.

Given the poor constraints on the planet's orbital eccentricity from archival data, Analyst Wong explored both circular and eccentric orbits by applying priors on the mid-eclipse time $t_{\rm sec}$ of varying widths. We found that regardless of the prior constraints on $t_{\rm sec}$, the best-fit eclipse timing was always tightly clustered around a consistent value roughly 0.003 d (∼4 minutes) after the circular-orbit prediction, with our posterior not being prior-dominated. For the fiducial fit, we applied a relatively wide uniform prior of $\mathcal{U}(2\,458\,573.58, 2\,458\,573.60)$ $\mathrm{BJD_{TDB}}$.

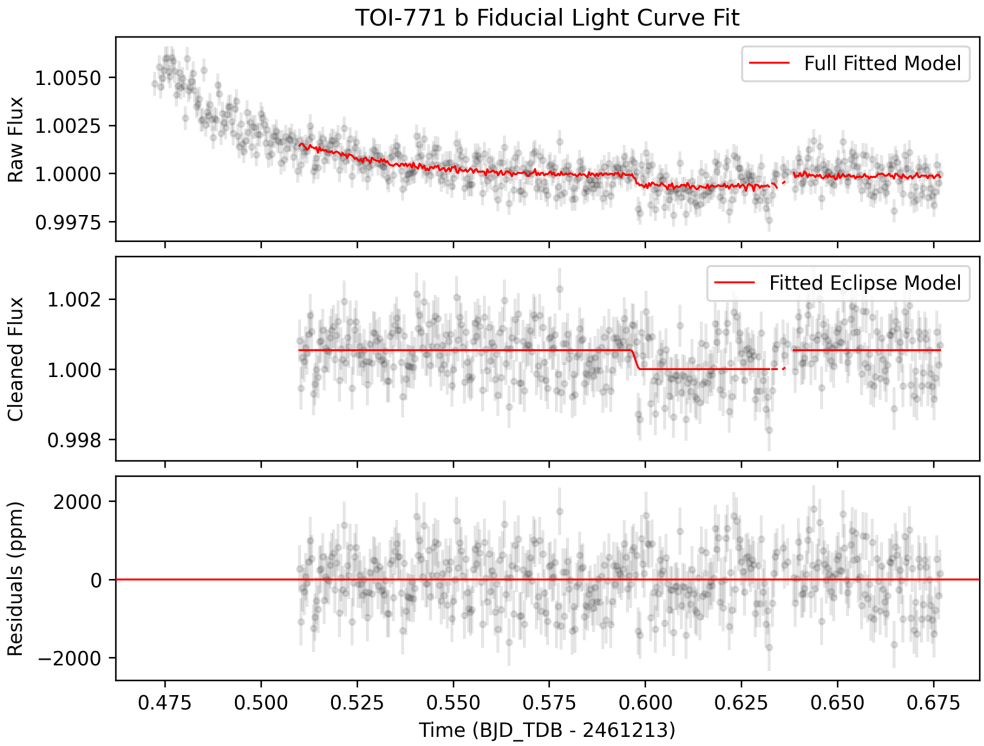

Figure 2: Fiducial light curve fit. *Top:* The raw, normalized flux measurements in black with the best fit combined systematics and eclipse model over-plotted in red. The first 100 integrations were not included in the fit. *Middle:* The systematics-divided flux measurements are shown in black, with the fitted eclipse model shown in red. *Bottom:* The "data − model" residuals. Residual time-correlated noise is apparent around the time of eclipse.

3.1 Results & Discussion

Analyst Wong selected a fiducial reduction and fit that yielded the smallest eclipse depth uncertainty, the results of which are presented in Table 2. The preferred light curve was extracted from a 4 px aperture, with the background annulus lying between 26 and 46 px from the centroid position. The measured eclipse depth is 539 ± 90 ppm. Figure 2 shows the fiducial light-curve fit, including the raw normalized photometric time series, the trimmed and systematics-corrected light curve, and the corresponding residuals. The standard deviation of the light curve residuals is 699 ppm, which is roughly 15% above the estimated stellar-photon-limited noise level.

The best-fit eclipse depth significantly exceeds the maximum expected eclipse depth of ∼390 ppm under the assumption of zero albedo and zero day-night recirculation. Overall, the significant correlated noise in the light curve raises the caveat that the results presented for this visit should be interpreted with caution. In particular, the noise may have a substantial biasing effect on both the mid-eclipse time and eclipse depth inferred from the light-curve fitting analysis. The source of this noise could not be easily identified.

Table 2: Fiducial eclipse fit results for TOI-771 b.

Eclipse Depth [ppm]	$t_{\rm sec}$ [BJD$_{\rm TDB}$]	Residual Std. Dev. [ppm]
539 ± 90	$2\,458\,573.5864^{+0.0015}_{-0.0011}$	699

4 Calibrated Stellar Flux Measurement

Following the methodology of Gordon et al. (2025), we measured absolutely-calibrated stellar photometry using the `calints` FITS files that we generated by downloading the Level 2 `rateints` from MAST and running them through Stage 2 of the JWST pipeline. Unlike in the data processing workflow used to derive the light curves for eclipse model fitting, we activated the `photom` step to obtain calibrated pixel flux values. The target flux was measured using a 5.69 px aperture and an 8.63–11.45 px background annulus, with an aperture correction factor of 1.497 applied. Adding in quadrature the observational scatter with the $\sigma(\mathrm{CF}) = 0.48\%$ and $\sigma(\mathrm{repeat}) = 0.45\%$ terms from Gordon et al. (2025), we obtained a calibrated stellar flux of 3.846 ± 0.025 mJy.

5 Discussion and Outlook

This report provides a **snapshot** of TOI-771 b from a single observation. Based on the significant correlated noise in the light curve in the vicinity of the predicted eclipse event and the higher-than-expected estimated eclipse depth, the results from the fiducial fit should be considered with caution. The inclusion of additional eclipses is needed to more accurately constrain the eclipse depth and timing. For community analysts, the reduction/fitting configurations and noise benchmarks presented here offer a practical starting point; for modelers, the preliminary depths/timings and robust stellar flux measurements enable early exploration of different atmospheric and/or surface scenarios.